A Study on the Interaction of DTPA Functionalised ZnO by Fluorescence Spectroscopy

Hetvi Dave [1], Naznin Shaikh [1], Harita Mehta [1], Padmaja Pamidimukkala [1,2]*

[1] Department of Chemistry, Faculty of Science, The Maharaja Sayajirao University of Baroda, Sayajigunj, Vadodara-390002

[2] Department of Environmental Studies, Faculty of Science, The Maharaja Sayajirao University of Baroda, Sayajigunj, Vadodara-390002

Email ID: padmaja.sudhakar-chem@msubaroda.ac.in

Received: 22.8.2025, Revised: 21.10.2025 Accepted: 24.10.2025

Abstract

Zinc Oxide (ZnO) nanoparticles find wide field applications in various areas including protein-molecule interactions. Green methods of synthesis which include hydrothermal synthesis techniques are gaining importance due to cost effectiveness and reduction in usage of toxic chemicals. Diethylene Triamine Pentaacetic Acid (DTPA) can be used for surface modification of metal oxides which can alter their properties. This work focusses on the synthesis of DTPA functionalised ZnO nanoparticles using microwave assisted hydrothermal synthesis method. The synthesised nanoparticles were characterised using UV-Visible spectroscopy, Fluorescence spectroscopy, Scanning Electron Microscopy (SEM), Fourier Transform Infrared Spectroscopy (FTIR), Powder X-Ray Diffraction Spectroscopy (P-XRD) and X-Ray Photoelectron Spectroscopy (XPS). The Bovine Serum Albumin (BSA) binding capacity of the nanoparticles was investigated and the Stern-Volmer constant (K_{sv}) of interaction was calculated as 7.93×10^6 M^{-1}. Further the effect of time on 'Protein Corona' system was studied.

1. Introduction

Metallic nanoparticles have been used in several medical applications like biosensing, bioimaging, sustained drug delivery, photoablation therapy and hyperthermia[1]. The metallic nanostructures are more useful as compared to the other nanomaterials due to the ability to control their dimensions, morphology, composition, and tunable optical properties. The functionalisation of nanoparticles with specific functional groups make them capable to bind to ligands, drugs and antibodies making them useful applicants in several biomedical

 DOI: 10.59143/isas.jisas.4.2.PSQM8496

applications[2]. Among the various nanoparticles, Zinc Oxide (ZnO) is extensively used because of its biocompatibility, biodegradability, ease of synthesis, low cost and easier functionalisation due to its -OH rich surface[3]. It finds many biomedical applications in drug delivery, biosensing, anticancer activity, wound healing, antimicrobial activity, etc. ZnO nanoparticles possess good luminescent properties. ZnO nanoparticles possess a band gap of 3.37 eV, exciton binding energy of 60 meV, high dielectric constant and Bohr exciton radius of ~2.34 nm[4,5]. The irradiation of ZnO with UV light causes promotion of an electron to the conduction band producing a hole in the valence band. These electron/hole pairs are responsible for the photochemical reactions generating Reactive Oxygen Species (ROS)[6].

ZnO nanoparticles are fluorescent because of the oxygen vacancies in them. The low stability of ZnO nanoparticles in aqueous media is due to their aggregation which leads to the quenching of their fluorescence thus hindering their use in biomedical applications. The aggregation of the nanoparticles can be overcome by their surface functionalisation[7]. However, ZnO nanoparticles release excess Zn^{2+} ions which cause cell death. This can be reduced by chelation of the metal oxides with a chelating agent. Chelating agents like Diethylene Triamine Pentaacetic Acid (DTPA), Ethylene Diamine Pentaacetic acid (EDTA), Citric acid, Oxalic acid, etc. when bound to the ZnO nanoparticles prevent the formation of excessive Zn^{2+} ions by stabilising the ZnO nanoparticles in the biological media[8]. DTPA is a broadly utilized metal chelating agent because it forms a stable complex with metals. Metal-chelate bonds are made through binding of the metal with the unshared pair of electrons on oxygen and nitrogen in DTPA, having a potential for eight coordination sites (from three nitrogen and five oxygen) facilitating further interface with organic molecules such as proteins[9,10,].

The most abundant protein available in the blood plasma is albumin. It plays a vital role in transport of drugs, its adsorption and viability. Bovine Serum Albumin (BSA) consists of 583 amino acids and is a water-soluble protein. BSA has structure homology with Human Serum Albumin (HSA) and is thus an extensively studied protein. The structure of BSA consists of three homologous domains (I, II and III). Each domain consists of two subdomains. The structure of albumin is primarily α-helical in nature. The hydrophobic pocket in domain II contains Tryptophan, Tyrosine and Phenylalanine amino acids. There are two tryptophan residues in BSA (Tryptophan-134 in domain I and Tryptophan-212 in domain II) which possess intrinsic fluorescence properties. Tryptophan-212 and

Tryptophan-134 are located in the hydrophobic binding pocket and on the surface of the molecule respectively[11].

ZnO is an amphoteric oxide which undergoes hydrolysis in water and forms a layer of hydroxide on the surface (Zn-OH) by adsorption of water molecules or biofluids causing agglomeration of the nanoparticles. The hydrodynamic size of the nanoparticles gets diminished in presence of negatively charged serum protein because of its adsorption on the nanoparticles and formation of protein corona[12].

To study the protein nanoparticle interactions, the adsorbed proteins can be broken down with fluorescence quenching. The fluorescence quenching is an effect that happens because of the protein binding to nanoparticles forming corona and subsequently losing its fluorescence. Changes in fluorescence of the nanoparticles are additionally demonstrative of the arrangement of protein corona, since the adsorption of proteins on nanoparticles results in quenching of the fluorescence of the nanoparticles[13,14].

Thus, this work focusses on the synthesis of DTPA functionalised ZnO nanoparticles prepared by microwave assisted hydrothermal synthesis which is a faster, cleaner and a green method for the synthesis of nanoparticles. The nanoparticles were optimised by fluorescence spectroscopy to find the optimum nanomaterial having highest emission intensity which was then further characterised using various analytical techniques and used for protein binding studies. The BSA binding capacity of the nanoparticles was investigated and the Stern-Volmer constant of interaction (K_{sv}) was calculated. Further the change in the fluorescence properties of BSA with time in presence of the nanoparticles (Protein Corona formation) was studied.

2. Experimental

2.1 Materials

Zinc Chloride ($ZnCl_2$) [M.W. of 136.286 g/mol], Diethylene Triamine Pentaacetic Acid (DTPA) [M.W. of 393.349 g/mol] were purchased from Spectrochem Pvt. Ltd. Bovine Serum Albumin (BSA) [M.W. of 66430.3 g/mol] and all other reagents used in this work were of analytical grade and were purchased from commercial suppliers. Deionized water was used for all the experiments.

2.2 Synthesis of DTPA functionalised ZnO nanoparticles

In a conical flask, 4.77 mmol of $ZnCl_2$ was weighed and dissolved in 50 mL deionised water. 0.25 mmol of DTPA was dissolved in ammonia (1:1) and added to the $ZnCl_2$

solution. Ammonia (1:1) was used for adjusting the pH to 10. The system was stirred for 15 minutes and then microwaved for different times, ranging from 1 minute to 10 minutes at intervals of 30 seconds to prepare the nanoparticles of varying microwave times. The contents were allowed to come to room temperature each time after microwaving for 30 seconds. It was then centrifuged at 10,000 rpm for 10 minutes. The particles were dried in oven for 24 hours. The DTPA functionalised ZnO nanoparticles prepared at different microwave times from 1 minute to 10 minutes were termed as ZnOD1m to ZnOD10m.

2.3 Optimisation of the nanoparticles by fluorescence spectroscopy

The synthesised nanoparticles were further characterized for their absorption and photoluminescence characteristics at excitation wavelength of 270 nm. The nanoparticle having highest fluorescence intensity was selected for further BSA binding studies.

2.4 Characterization

The UV-Visible spectrum was recorded using Lambda 35 UV/Vis Spectrometer. Jasco FP-6300 Spectrofluorometer was used to record fluorescence spectra. The morphology of the nanoparticles was identified by Scanning Electron Microscopy (SEM) using JEOL (JSM-7600F). The Fourier Transform Infrared Spectroscopy (FTIR) analysis was done using Bruker ALPHA-T IR spectrometer. The crystallinity and particle size were determined by Powder X-Ray Diffraction Spectroscopy (P-XRD) using Bruker D8 Advance spectrometer. The X-Ray Photoelectron Spectroscopy (XPS) analysis was conducted using Physical Electronic PHI 5000 VersaProbe III.

2.5 Investigation of BSA binding capacity of DTPA functionalised ZnO nanoparticles

To investigate the maximum amount of BSA that can effectively be adsorbed on the DTPA functionalised ZnO nanoparticles, 1 mL of varying concentrations (0.0 ppm to 150 ppm) of BSA solution were added to 2 mL 0.2 mg ZnOD2m and fluorescence was measured at excitation wavelength of BSA (280 nm). From this study, the maximum amount of BSA that can be adsorbed on the nanoparticles was determined.

2.6 Effect of time on BSA bound ZnOD2m (Protein Corona) system

The effect of time on protein corona complex was studied by adding 4 mg ZnOD2m to 25 mL 10 ppm BSA solution and stirring. After every 30 minutes, the contents were centrifuged and change in fluorescence of the supernatant liquid was measured at excitation wavelength of BSA (280 nm).

3. Results and Discussion

3.1 Optimisation of the nanoparticles

Fig. 1a shows the fluorescence spectra of the prepared nanoparticles (ZnOD1m to ZnOD10m) excited at 270 nm. The peak at 300 nm could be due to the band gap transition of ZnO. The emission peak observed at 330 nm could be ascribed to the -OH terminations which confirmed the formation of -OH passivated ZnO nanoparticles. The broad peak observed at ~400 nm was attributed to the strong interactions of -OH groups with surface zinc defects. The peak observed at 470 nm was attributed to the oxygen vacancy defects. Further it was observed that with the increase in microwave time for preparation of the nanoparticles, the fluorescence peak observed at 330 nm was quenched suggesting the destruction of -OH terminal groups and hydrogen bonding[15]. Thus, the DTPA functionalised ZnO nanoparticles prepared at 2 minutes microwave time (ZnOD2m) was optimum and was further used for investigating its interaction with BSA.

3.2 Characterization

3.2.1 UV-Visible spectroscopy

Fig. 1b shows the absorption spectrum of ZnOD2m nanoparticles. It showed a maximum absorbance at 270 nm due to the intrinsic band gap absorption in ZnO. The shift of the absorption peak to shorter wavelength as compared to the bulk indicates that the particles are of nanoscale. The absorption band at 366 nm could be attributed to the band-to-band transition from valence band to conduction band ($O_{2p} \rightarrow Zn_{3d}$)[16,17].

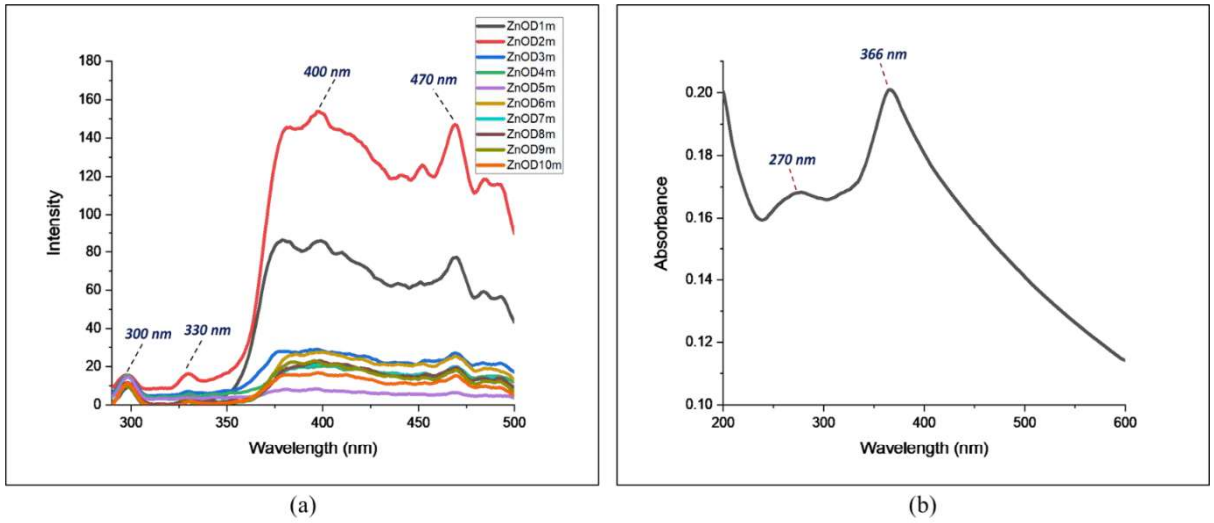

Fig. 1: (a) Fluorescence spectra of ZnOD1m to ZnOD10m and (b) Absorption spectrum of the optimised nanoparticle (ZnOD2m)

3.2.2 SEM analysis

The morphology of ZnOD2m was determined using SEM. Fig. 2a suggested that the nanoparticles formed were amorphous and porous in nature with uniform particle distribution. The large number of ZnO crystallites finally arranged to a nonporous uniform structure as seen in Fig. 2b.

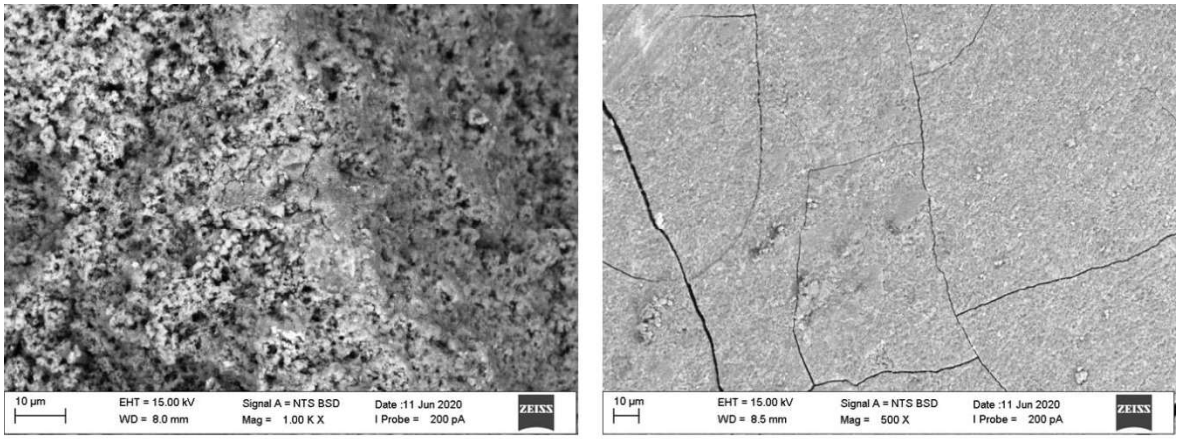

(a) (b)

Fig. 2: SEM images of ZnOD2m

3.2.3 FTIR analysis

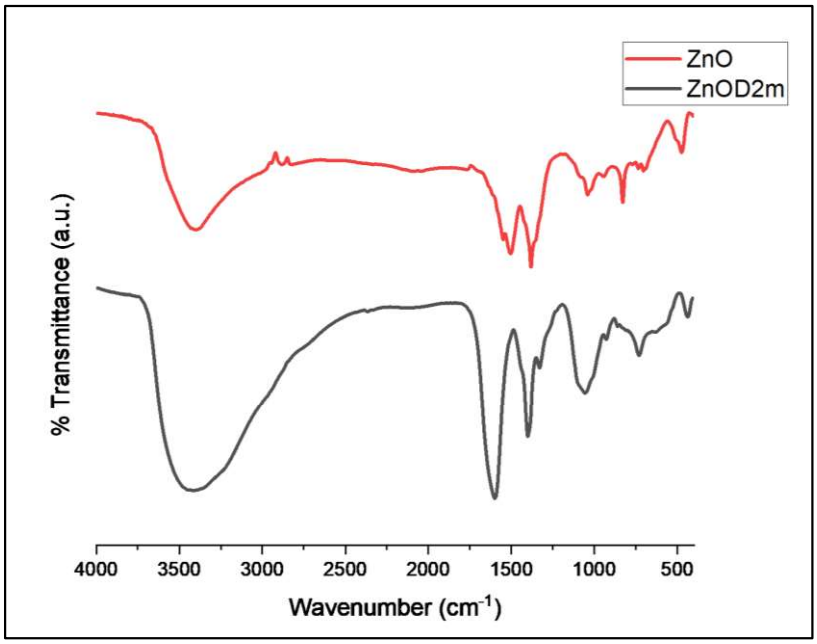

Fig. 3: FTIR of ZnO and ZnOD2m

The FTIR spectrum of ZnO and ZnOD2m are depicted in Fig. 3. The peak corresponding to the transverse stretching modes of Zn-O were observed at 478 cm^{-1} and 693 cm^{-1} which shifted to 438 cm^{-1} and 632 cm^{-1} in ZnOD2m. The peak due to the out of plane -OH bending was observed at 780 cm^{-1} in ZnO shifted to 731 cm^{-1} in ZnOD2m. The peaks

observed at 3401 and 3418 cm^{-1} respectively in ZnO and ZnOD2m were attributed to -OH stretching vibrations[18,19].

An additional peak corresponding to the C-N stretching vibrations was observed at 1056 cm^{-1} in ZnOD2m. Further, the peaks observed at 1330 cm^{-1} and 1400 cm^{-1} corresponded to the C-O asymmetric stretching and C-O symmetric stretching vibrations respectively of DTPA. The peak observed at 1599 cm^{-1} corresponded to the C=O stretching of carboxyl group of DTPA.

The additional C-N stretching, C-O asymmetric stretching, C-O symmetric stretching and C=O stretching vibrations observed in ZnOD2m confirmed the successful binding of DTPA and ZnO through amino and carboxyl groups of DTPA.

3.2.4 P-XRD

The synthesised nanoparticles were subjected to X-Ray diffraction studies. Fig. 4 show the P-XRD pattern of ZnO and ZnOD2m. The diffraction peaks were observed at 2θ = 31.80º, 34.52º, 36.34º, 47.59º, 56.62º, 62.77º, 66.47º, 67.45º, 68.90º, 72.44º and 77.01º for ZnO while for ZnOD2m the diffraction peaks were observed at 2θ values of 31.86°, 34.57°, 36.37°, 47.63°, 56.66°, 62.83°, 66.86°, 67.92°, 68.99°, 72.59º and 77.04° which corresponded to (100), (002), (101), (102), (110), (103), (200), (112), (201), (004) and (202) diffraction planes of ZnO indicating hexagonal wurtzite structure of the ZnO nanoparticles. The small positive shift in the 2θ values observed in ZnOD2m as compared to ZnO was attributed to chelation and surface modification of ZnO by DTPA which could affect the lattice structure of ZnO by inducing compression strain and a resultant decrease in interplanar spacing[20]. The average particle size was found to be 28.52 and 22.03 nm for ZnO and ZnOD2m respectively using the Debye-Scherrer equation (Equation 1)-

$$D = \frac{K\lambda}{\beta cos\theta} \qquad (1)$$

Where D is the average crystallite size of the nanoparticles, K is the Scherrer constant equal to 0.9, λ is the wavelength of X-ray beam (1.54 Å), β is the Full Width at Half Maximum (FWHM) of the diffraction peak and θ is the Bragg angle of diffraction peak[21].

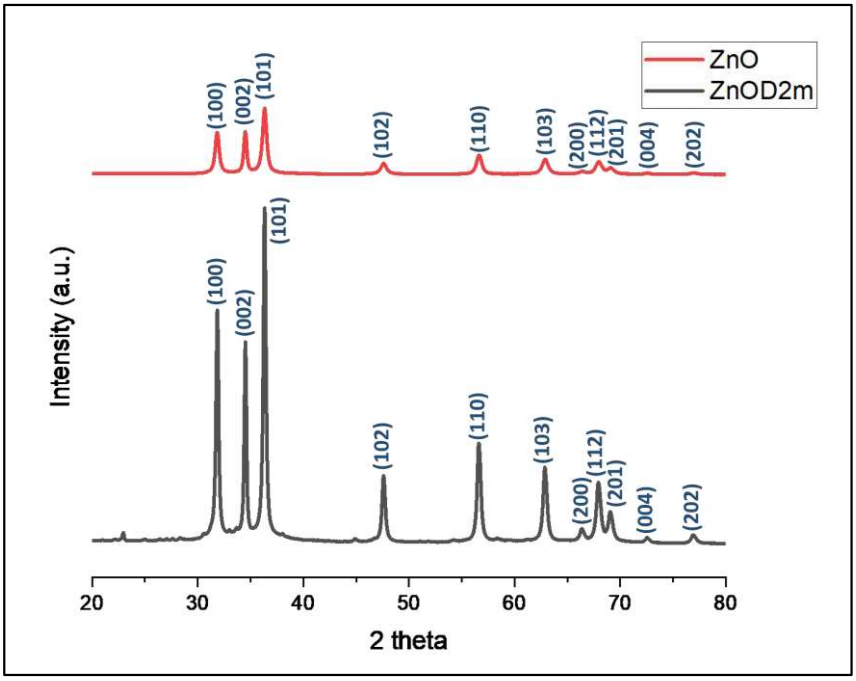

Fig. 4: P-XRD of ZnO and ZnOD2m

3.2.5 XPS analysis

The XPS survey spectrum of ZnOD2m is depicted in Fig. 5a. The deconvoluted XPS spectrum of Zn2p state (Fig. 5b) exhibited peaks at 1019 eV and 1042.10 eV corresponding to the Zn2p1/2 and Zn2p3/2 states of zinc respectively. The binding energy difference of ~23 eV confirmed the presence of zinc as Zn (II). The deconvoluted O1s spectrum (Fig. 5c) depicted a peak at 527.99 eV due to the oxygen$^-$ ions present in the lattice of ZnO. The peak observed at 528.67 eV was attributed to the oxygen vacancies while that observed at 529.60 was attributed to the surface adsorbed oxygen and hydroxyl groups[22]. The deconvoluted C1s spectrum (Fig. 5d) showed three peaks. The peak at 281.58 eV was due to the C-C bonds in DTPA. The peak observed at 283.03 eV corresponded to the C-O bonds while the peak observed at 285.46 eV was due to the C=O bonds[23]. The deconvoluted N1s XPS spectrum (Fig. 5e) showed three peaks due to the N-Zn bonds and different bonding configurations of nitrogen with zinc at 395.81 eV, 397.16 eV and 398.47 eV[24].

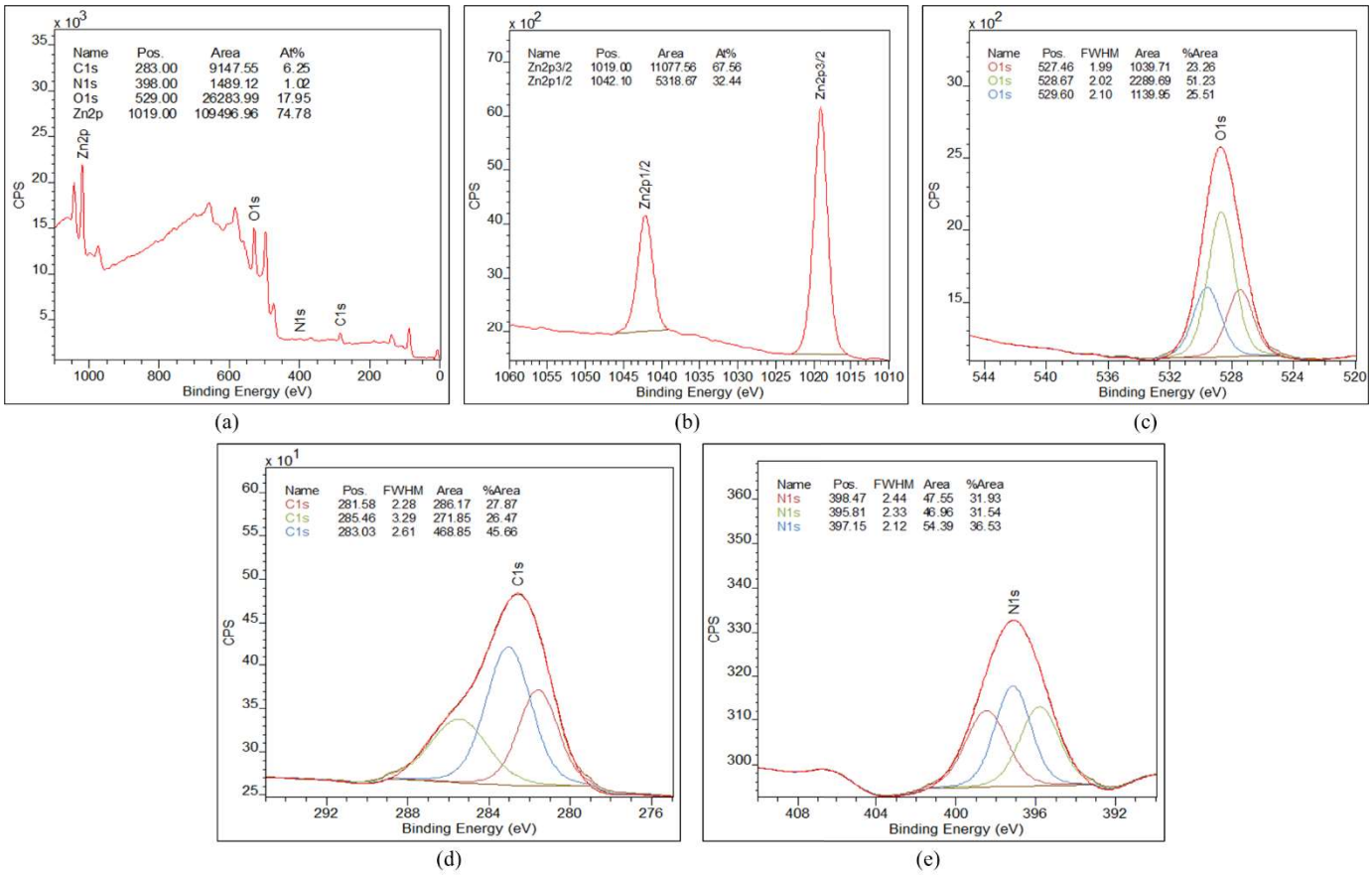

Fig. 5: (a) XPS Survey spectrum; (b) Zn2p XPS spectrum; (c) O1s XPS spectrum; (d) C1s XPS spectrum and (e) N1s XPS spectrum of ZnOD2m

3.3 Investigation of BSA binding capacity of DTPA functionalised ZnO nanoparticles

The fluorescence spectra of ZnOD2m on addition of BSA (Fig. 6a) showed that the intensity of peak at 330 nm increased on addition of varying concentrations of BSA upto 60 ppm. Also, a decrease in fluorescence intensity at 370 nm and 470 nm was observed. The higher stokes shift was related to the enhancement of exciton localization in smaller particles of ZnO stabilized by BSA. At higher concentration of BSA the emission of ZnO was completely quenched[25]. The Stern-Volmer constant (K_{sv}) of interaction was calculated using the formula (Equation 2):

$$\frac{F}{Fo} = 1 + Ksv[A] \qquad (2)$$

Where F_o is the fluorescence intensity in absence of BSA, F is the fluorescence intensity in presence of BSA, K_{sv} is the Stern-Volmer interaction constant of interaction and [A] is the concentration of analyte BSA. Fig. 6b shows the Stern-Volmer plot showing the interaction between BSA and the nanoparticles. The K_{sv} was calculated to be 7.93×10^6 M^{-1} which

suggests efficient complexation between BSA and ZnOD2m resulting in quenching of fluorescence.

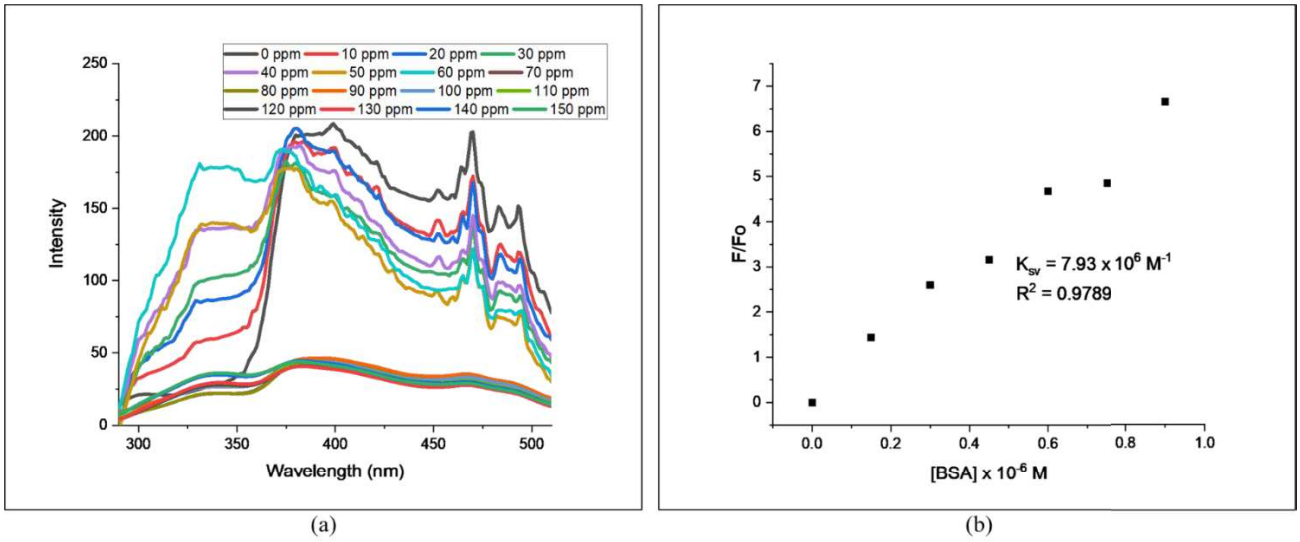

Fig. 6: (a) Fluorescence emission of ZnOD2m with varying concentration of BSA and (b) Stern-Volmer plot for interaction between BSA and ZnOD2m

3.4 Effect of time on BSA bound ZnOD2m (Protein Corona) system

Protein coatings can cause a change in the surface properties of the nanoparticles. It has been established that protein coatings are not static entities. They undergo continuous adsorption and desorption in which originally adsorbed protein desorbs and other adsorbs. The hard corona consists proteins having high affinity for the nanoparticles. This results in the formation of a strong and tight bonding between the nanoparticles and protein leading to the formation of a more stable complex. On the other hand, soft corona is constituted by the proteins having lower affinity for the nanoparticles and thus take more time for the formation. From a physicochemical point of view, the adsorption and desorption of protein can be interpreted in the form of a chemical reaction as (Equation 3)-

$$P + nS \leftrightarrow PnS \quad (3)$$

where P is the protein binding to the adsorbent (nanoparticle) S, n is the binding sites of the adsorbent and PnS is the protein corona formed[26,27].

The fluorescence quenching is an effect that occurs due to the protein binding to the nanoparticles i.e., protein corona formation thus losing its fluorescence. On centrifugation the soft corona or the loosely bound proteins will be present in the supernatant liquid and can be separated from the protein corona complex and detected by studying the fluorescence of the supernatant liquid. It was observed that the fluorescence of BSA did not change with time in absence of ZnOD2m (Fig. 7a). While in presence of ZnOD2m (Fig. 7b), the

fluorescence intensity at 330 nm was observed to decrease with time on interaction between BSA and ZnOD2m.

Thus, fluorescence of proteins is an interesting parameter, since the adsorption of proteins on nanoparticles usually leads to quenching of the native fluorescence of proteins. Upon formation of protein corona complex in case of intrinsically fluorescent nanoparticles, the fluorescence of nanoparticles can be quenched while in case of fluorescent proteins, the fluorescence of the protein can be quenched.

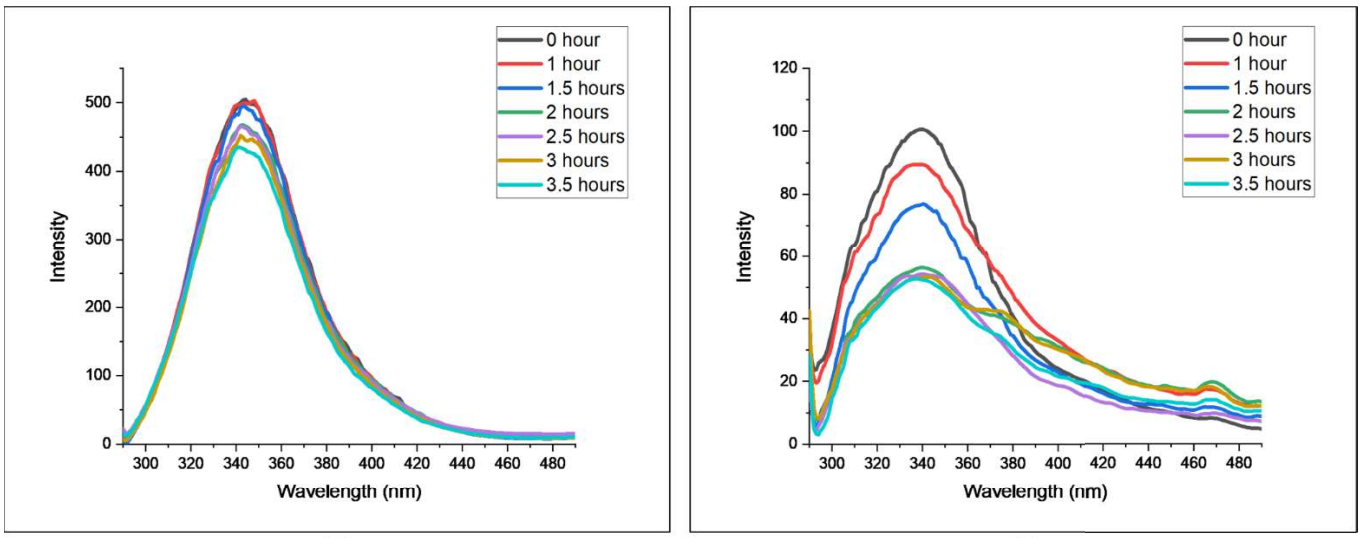

Fig. 7: Quenching of 10 ppm BSA in (a) absence and (b) presence of ZnOD2m

Conclusion

DTPA functionalised ZnO nanoparticles were successfully synthesised using microwave assisted hydrothermal synthesis technique which is a green method for the synthesis of nanoparticles. Fluorescence studies revealed that the nanoparticles synthesised at 2 minutes microwave time showed the maximum fluorescence intensity and were further used for BSA binding studies. The nanoparticles were amorphous and porous in nature with uniform particle distribution. The BSA binding studies revealed the Stern Volmer constant (K_{sv}) of interaction between BSA and ZnOD2m to be 7.93×10^6 M^{-1}. On addition of BSA to the nanoparticles, the fluorescence intensity was observed to decrease which confirmed the binding of BSA to the nanoparticles (protein corona formation).

Authors' Contributions: Hetvi Dave : Formal analysis, Investigation, Original draft preparation

Naznin Shaikh : Methodology, project administration, Original draft preparation

Harita Mehta : Formal Analysis, Investigation, writing, Original draft preparation

Padmaja Pamidimukkala: Conceptualization, Methodology, project administration, supervision, validation, writing-review & Eiting

Conflict of interest: The authors declare that they have no known competing financial interests or personal relationships that could have appeared to influence the work reported in this paper.

Acknowledgement

One of the authors (Hetvi Dave) is thankful to DST-INSPIRE (Fellowship no. IF200319) for providing the financial assistance. The authors are thankful to Solvay India R&I Centre, Vadodara, Gujarat for SEM analysis and SAIF IIT Roorkee for P-XRD and XPS analysis.

References

1. R. Khursheed, K. Dua, S. Vishwas, M. Gulati, N.K. Jha, G.M. Aldhafeeri, F.G. Alanazi, B.H. Goh, G. Gupta, K.R. Paudel, P.M. Hansbro, D.K. Chellappan, S.K. Singh, Biomedical applications of metallic nanoparticles in cancer: Current status and future perspectives, Biomed. Pharmacother., 150, 112951-112975, 2022.
2. M.T. Yaraki, S. Zahed Nasab, I. Zare, M. Dahri, M. Moein Sadeghi, M. Koohi, Y.N. Tan, Biomimetic Metallic Nanostructures for Biomedical Applications, Catalysis, and beyond, Ind. Eng. Chem. Res., 61, 7547–7593, 2022.
3. Y. Sun, W. Zhang, Q. Li, H. Liu, X. Wang, Preparations and applications of zinc oxide based photocatalytic materials, Adv. Sens. Energy Mater., 2, 100069-100087, 2023.
4. N. J, K. E, R. S, Green Synthesis of Zinc Oxide Nanoparticles: Eco-Friendly Advancements for Biomedical Marvels, Resour. Chem. Mater., 3, 294–316, 2024.
5. S. Anjum, M. Hashim, S.A. Malik, M. Khan, J.M. Lorenzo, B.H. Abbasi, C. Hano, Recent Advances in Zinc Oxide Nanoparticles (ZnO NPs) for Cancer Diagnosis, Target Drug Delivery, and Treatment, Cancers (Basel)., 13, 4570-4600, 2021.
6. M. Martínez-Carmona, Y. Gun'Ko, M. Vallet-Regí, Zno nanostructures for drug delivery and theranostic applications, Nanomaterials, 8, 1–27, 2018.
7. J. Wang, R. Chen, L. Xiang, S. Komarneni, Synthesis, properties and applications of ZnO nanomaterials with oxygen vacancies: A review, Ceram. Int., 44, 7357–7377, 2018.
8. M.P. Cuajungco, M.S. Ramirez, M.E. Tolmasky, Zinc: Multidimensional effects on

living organisms, Biomedicines, 9, 1–26, 2021.

9. P. Yudaev, E. Chistyakov, Chelating Extractants for Metals, Metals (Basel)., 12, 1275-1334, 2022.
10. M. Parhizgar Keradeh, S.A. Tabatabaei-Nezhad, A comprehensive evaluation of the effect of key parameters on the performance of DTPA chelating agent in modifying sandstone surface charge, Heliyon, 9, e21990-22008, 2023.
11. D. Agudelo, P. Bourassa, J. Bruneau, G. Bérubé, É. Asselin, H.A. Tajmir-Riahi, Probing the binding sites of antibiotic drugs doxorubicin and N-(trifluoroacetyl) doxorubicin with human and bovine serum albumins, PLoS One, 7, 1–13, 2012.
12. H. Hematian, B. Rezek, Study of bovine serum albumin interaction with zinc oxide surfaces by force field simulations, IOP Conf. Ser. Mater. Sci. Eng., 1050, 012006-012011, 2021.
13. S. Dominguez-Medina, L. Kisley, L.J. Tauzin, A. Hoggard, B. Shuang, A.S. D. S. Indrasekara, S. Chen, L.Y. Wang, P.J. Derry, A. Liopo, E.R. Zubarev, C.F. Landes, S. Link, Adsorption and Unfolding of a Single Protein Triggers Nanoparticle Aggregation, ACS Nano, 10, 2103–2112, 2016.
14. S.E. Cornwell, S.O. Okocha, E. Ferrari, Multivariate Analysis of Protein–Nanoparticle Binding Data Reveals a Selective Effect of Nanoparticle Material on the Formation of Soft Corona, Nanomaterials, 13, 2901-2911, 2023.
15. G. Jain, C. Rocks, P. Maguire, D. Mariotti, One-step synthesis of strongly confined, defect-free and hydroxy-terminated ZnO quantum dots, Nanotechnology, 31, 215707-215715, 2020.
16. Z. Chen, Q. Gao, M. Ruan, J. Shi, Zinc oxide nanoarrays in nanoporous nickel phosphate with a huge blueshift ultraviolet-visible exciton absorption peak, Appl. Phys. Lett., 87, 093113–093116, 2005.
17. L. Garcés, C.R. Garcia, V. Rodriguez-Gonzalez, D.Y. Medina-Velazquez, J. Oliva, Tuning the emission color and enhancement of the NIR emission of ZnO:Ca phosphors with the Ca concentration, Ceram. Int., 48, 17885–17892, 2022.
18. C.R. Rajith Kumar, V.S. Betageri, G. Nagaraju, G.H. Pujar, H.S. Onkarappa, M.S. Latha, Synthesis of Core/Shell (ZnO/Ag) Nanoparticles Using Calotropis gigantea and Their Applications in Photocatalytic and Antibacterial Studies, J. Inorg. Organomet. Polym. Mater., 30, 3410–3417, 2020
19. V.L. Silva, R. Carvalho, M.P. Freitas, C.F. Tormena, W.C. Melo, Spectrometric and

theoretical investigation of the structures of Cu and Pb/DTPA complexes, Struct. Chem., 18, 605–609, 2007.

20. X. Yang, Y. Wang, X. Tong, N. Yang, Strain Engineering in Electrocatalysts: Fundamentals, Progress, and Perspectives, Adv. Energy Mater. 12, 2102261-2102300, 2022.
21. G. Otis, M. Ejgenberg, Y. Mastai, Solvent-free mechanochemical synthesis of zno nanoparticles by high-energy ball milling of ε-$Zn(OH)_2$ crystals, Nanomaterials 11, 1–12, 2021.
22. M. Tomić, M. Claros, I. Gràcia, E. Figueras, C. Cané, S. Vallejos, Zno structures with surface nanoscale interfaces formed by Au, Fe_2O_3, or Cu_2O modifier nanoparticles: Characterization and gas sensing properties, Sensors, 21, 4509-4532,2021.
23. M. Kwoka, A. Kulis-Kapuscinska, D. Zappa, E. Comini, J. Szuber, Novel insight on the local surface properties of ZnO nanowires, Nanotechnology, 31, 465705-465714, 2020.
24. A. Ievtushenko, O. Khyzhun, I. Shtepliuk, V. Tkach, V. Lazorenko, G. Lashkarev, X-ray photoelectron spectroscopy study of nitrogen and aluminum-nitrogen doped ZnO films, Acta Phys. Pol. A, 124, 858–861, 2013.
25. A. Kathiravan, G. Paramaguru, R. Renganathan, Study on the binding of colloidal zinc oxide nanoparticles with bovine serum albumin, J. Mol. Struct., 934, 129–137, 2009.
26. P.C. Ke, S. Lin, W.J. Parak, T.P. Davis, F. Caruso, A Decade of the Protein Corona, ACS Nano, 11, 11773–11776, 2017.
27. E.G. Solveyra, D.H. Thompson, I. Szleifer, Proteins Adsorbing onto Surface-Modified Nanoparticles: Effect of Surface Curvature, pH, and the Interplay of Polymers and Proteins Acid–Base Equilibrium, Polymers (Basel)., 14, 112951-112975, 2022.